OMAE2018-78067

NON-LINEAR SIMULATION OF A WAVE ENERGY CONVERTER WITH MULTIPLE DEGREES OF FREEDOM USING A HARMONIC BALANCE METHOD

Riccardo Novo
Giovanni Bracco
Sergej A. Sirigu
Giuliana Mattiazzo
Politecnico di Torino,
Dipartimento di Ingegneria Meccanica e Aerospaziale,
C.so Duca degli Abruzzi, 24, 10129 Torino
Italy

Alexis Mérigaud[*]
John V. Ringwood
Maynooth University
Centre for Ocean Energy Research
Dpt. of Electronic Engineering
Maynooth, co. Kildare
Ireland
Email: alexis.merigaud.2015@mumail.ie

ABSTRACT

Computationally efficient simulation methods for wave energy converters (WECs) are useful in a variety of applications. The simulation task is particularly challenging when non-linearities are present in the WEC model. Using a Fourier projection of the system inputs and variables, harmonic balance (HB) is a computationally-efficient method to solve for the steady-state motion of a non-linear system, preserving an accurate representation of the non-linear effects. In previous work, HB has been used for the simulation of WECs with one degree of freedom (DoF). Here, HB is presented for WEC systems with an arbitrary number of DoFs. A non-linear, 2-DoF model of the ISWEC wave energy device is used as an example of application. The HB implementation of the ISWEC model is described in detail. Through numerical applications, chosen in both regular and irregular waves, general features of the HB method are exemplified, in particular the exponential convergence rate to the actual mathematical solution, and the sensitivity, in some cases, to the starting point of the HB algoritm.

1 INTRODUCTION

Computationally efficient simulation methods are desirable in wave energy applications, for tasks involving extensive numerical simulations, such as power assessment, design optimi-

sation, or fatigue analysis [1]. For such tasks, semi-analytical WEC models, based on linear hydrodynamic theory, are commonplace [1].

When the WEC physical model is linear, frequency-domain simulations are adequate. However, non-linear dynamical effects can be significant, especially under controlled conditions [2], and therefore should be included in the physical description of the WEC where appropriate. Such dynamical non-linearities can be related to the hydrodynamic interactions (viscous dissipation, non-linear geometry, etc.), to mooring line effects, or to the power take-off (PTO) system.

The presence of non-linearities makes it impossible to use the common frequency-domain approach to compute the device response, and therefore, time-domain numerical integration schemes are usually employed [1], which are significantly slower than linear frequency-domain calculations. In particular, a major computational burden comes from the computation of linear radiation forces, expressed as a convolution product between the radiation impulse-response kernel, and the past values of the device velocity [3]. The convolution can be avoided by approximating the radiation forces by means of a state-space representation, with the effects of increasing the system dimension, and inducing possible inaccuracies. It is suggested in [3] that state-space approximations can reduce the computation time by 20 to 80 times, with respect to the direct computation of the convolution integral.

Other approaches avoid time-domain integration. For exam-

---
[*]Address all correspondence to this author.

ple, statistical linearisation, quadratisation or cubicisation could be used, whereby, through an iterative process, the non-linear forces are approximated with, respectively, linear, quadratic and cubic functions. The optimal approximation depends on the sea state. So far, only statistical linearisation has been applied to WEC modelling [4]. Although very computationally efficient [1, 5], statistical linearisation has limited accuracy, especially when it comes to analysing the WEC trajectory in the time domain [5].

Alternatively, a harmonic balance (HB) method has been proposed in [5] for WEC simulation. The approach, termed *non-linear frequency-domain* in [5], relies on a projection of the dynamical equations onto a Fourier basis, to determine the WEC steady-state response in a periodic excitation signal. HB has been widely used for the simulation of strongly non-linear electric circuits [6, 7]. By separating the linear terms (which include memory terms) from the non-linear terms (which are usually memoryless), the method handles the linear terms efficiently and accurately in the frequency domain, while preserving a realistic representation of the non-linear effects. So far, in the wave energy field, the approach has only been detailed and validated with WECs with one degree of freedom (DoF) [5, 8]. In this paper, the method is presented for WEC systems with an arbitrary number of DoFs.

Note that the HB method is suitable for the study of "smooth" non-linear effects [8]. For discontinuous motions or forces, such as those which occur with Coulomb-damping-type effects, or with snap loads on moorings or wave slams, a problem parametrisation using other types of (possibly discontinuous) basis functions should be investigated. Therefore the study of extreme or discontinuous events is out of the scope of this study.

Numerical examples are shown, based on a 2-DoF model of the ISWEC, a wave energy device developed at Politecnico di Torino [9, 10]. The applicability of the method is investigated in both regular and irregular waves, and a comparison with a 2nd-order Runge-Kutta (RK2) integration is provided to better understand the advantages and limitations of the HB approach.

The harmonic balance method applied to a WEC system with multiple DoFs is detailed in Section 2 for a WEC with multiple DoFs. Section 3 describes the physical model of the ISWEC device, and Section 4 briefly explains how it can be reformulated as a HB problem. Simulation results are shown in Section 5, for regular and irregular wave excitation. Finally, conclusions are presented in Section 6.

2 HARMONIC BALANCE METHOD FOR WECS WITH MULTIPLE DEGREES OF FREEDOM
2.1 Dynamical equations

The WEC[1] generalised coordinates and their time derivatives are denoted, respectively, $\mathbf{x}$, $\dot{\mathbf{x}}$ and $\ddot{\mathbf{x}}$, which are all vector-valued functions defined on the simulation time interval $[0; T]$, and taking values in $\mathbb{R}^D$, where D is the number of DoFs. For a large class of WEC models, the dynamical equations can be written as follows, for $t \in [0; T]$:

$$\mathscr{L}[\mathbf{x}](t) + \mathscr{N}[\mathbf{x}](t) - \mathbf{e}(t) = 0_{\mathbb{R}^D} \tag{1}$$

where $\mathscr{L}$ and $\mathscr{N}$ are, respectively, linear and non-linear operators, with $\mathscr{L}[\mathbf{x}](t) \in \mathbb{R}^D$ and $\mathscr{N}[\mathbf{x}](t) \in \mathbb{R}^D$, while $\mathbf{e}(t) \in \mathbb{R}^D$ represents an external excitation signal (typically, linear wave excitation forces or moments). Not all components of Eqn. (1) may represent hydrodynamic interactions. Instead, some of them may express internal dynamics, which are not directly affected by the fluid-structure interaction, and therefore the corresponding components of $\mathbf{e}(t)$ may be uniformly zero in $[0; T]$.

$\mathscr{N}$ is assumed to be a memoryless operator, so that:

$$\mathscr{N}[\mathbf{x}](t) = \mathbf{g}(\mathbf{x}(t), \dot{\mathbf{x}}(t), \ddot{\mathbf{x}}(t)) \tag{2}$$

for some non-linear function $\mathbf{g}$ from $\mathbb{R}^D \times \mathbb{R}^D \times \mathbb{R}^D$ to $\mathbb{R}^D$. Note that a non-linear forcing term could be included in $\mathscr{N}$, without changing the rest of the derivations presented in this paper. For example, Eqn. (2) could be modified as $\mathscr{N}[\mathbf{x}](t) = \mathbf{g}(\mathbf{x}(t), \dot{\mathbf{x}}(t), \ddot{\mathbf{x}}(t), \eta(t))$, where η is the wave elevation at the WEC location. However, this possibility is omitted here for the sake of simplicity.

Further, the linear operator $\mathscr{L}$ can be split into a memoryless part, $\mathscr{L}_{ml}$, and a causal, linear convolution operator, $\mathscr{L}_c$, so that $\mathscr{L} = \mathscr{L}_{ml} + \mathscr{L}_c$. The memoryless operator $\mathscr{L}_{ml}$ is expressed as:

$$\mathscr{L}_{ml}[\mathbf{x}](t) = M\ddot{\mathbf{x}}(t) + C\dot{\mathbf{x}}(t) + S\mathbf{x}(t) \tag{3}$$

where $M \in \mathbb{R}^{D \times D}$ is the inertia matrix of the system, $C \in \mathbb{R}^{D \times D}$ is a linear damping matrix, and $S \in \mathbb{R}^{D \times D}$ is a linear stiffness matrix. In the formulation of Eqn. (3), C or S may be zero: for example, $S = 0$ if all the stiffness terms are non-linearly modelled.

The convolution operator, $\mathscr{L}_c$, is assumed to act on the device velocity only:

$$\mathscr{L}_c[\mathbf{x}](t) = \int_0^\infty K(\tau)\dot{\mathbf{x}}(t - \tau)d\tau \tag{4}$$

———————

[1] Although, for conciseness, the term "WEC" is employed in this section, the formulation developed applies equally well to individual WECs and WEC farms.

where $K \in \mathbb{R}^{D \times D}$ is a causal, matrix-valued impulse-response function. Typically, the convolution integral of Eqn. (4) represents the memory terms of the hydrodynamic radiation forces and moments [11]. Thus, for those rows of Eqn. (1) which do not express hydrodynamic interactions, and for those components of **x** which are not hydrodynamic DoFs, the corresponding rows and columns of $K(\tau)$ may be zero. In contrast, the non-zero rows and columns of $K(\tau)$ form $K_{\text{rad}}(\tau) \in \mathbb{R}^{D_\text{h} \times D_\text{h}}$, the radiation impulse response kernel of the system, where D_h is the number of hydrodynamic DoFs.

Note, finally, that $\mathscr{L}_{ml}$ could also be expressed using convolution operators acting on **x** and its derivatives, with $K_1(\tau) = M\delta(\tau)$, $K_2(\tau) = C\delta(\tau)$ and $K_3(\tau) = S\delta(\tau)$. However, it is useful in the rest of this paper to separate the memory-less terms from the memory terms.

2.2 The harmonic balance approach

Let us now consider the steady-state solution of Eqn. (1), when the WEC is subject to a periodic excitation signal $\mathbf{e}(t)$ with period T, described as a finite sum of harmonic sinusoids:

$$\mathbf{e}(t) = \hat{\mathbf{e}}_0 + \sum_{k=1}^{N} \hat{\mathbf{e}}_{2k-1} \cos(\omega_k t) + \hat{\mathbf{e}}_{2k} \sin(\omega_k t) \quad (5)$$

where $\forall k \in [\![1; N]\!]$, $\omega_k = k\omega_1$, $\omega_1 = \frac{2\pi}{T}$, and the component amplitudes $\hat{\mathbf{e}}_{2k-1}$ and $\hat{\mathbf{e}}_{2k} \in \mathbb{R}^D$ are derived from the wave excitation spectrum at frequency ω_k. Define

$$\hat{\mathbf{e}} := \begin{pmatrix} \hat{\mathbf{e}}_0 \\ \vdots \\ \hat{\mathbf{e}}_{2N} \end{pmatrix} \in \mathbb{R}^{(2N+1)D} \quad (6)$$

The harmonic balance method solves for the first N harmonics of the steady-state solution **x**, which is then approximated as:

$$\mathbf{x}(t) \approx \hat{\mathbf{x}}_0 + \sum_{k=1}^{N} \hat{\mathbf{x}}_{2k-1} \cos(\omega_k t) + \hat{\mathbf{x}}_{2k} \sin(\omega_k t) \quad (7)$$

so that the unknown variables are entirely characterised by:

$$\hat{\mathbf{x}} := \begin{pmatrix} \hat{\mathbf{x}}_0 \\ \vdots \\ \hat{\mathbf{x}}_{2N} \end{pmatrix} \in \mathbb{R}^{(2N+1)D} \quad (8)$$

$\dot{\hat{\mathbf{x}}}$ and $\ddot{\hat{\mathbf{x}}}$ are obtained as $\dot{\hat{\mathbf{x}}} = \Omega \hat{\mathbf{x}}$ and $\ddot{\hat{\mathbf{x}}} = \Omega^2 \hat{\mathbf{x}}$, where $\Omega \in$

$\mathbb{R}^{(2N+1)D \times (2N+1)D}$ is block-diagonal:

$$\Omega = \begin{pmatrix} \Omega_0 & & 0 \\ & \ddots & \\ 0 & & \Omega_N \end{pmatrix} \quad (9)$$

with $\Omega_0 = 0_{\mathbb{R}^{D \times D}}$, and

$$\Omega_k = \begin{pmatrix} 0_{\mathbb{R}^{D \times D}} & \omega_k \mathbb{I}_{\mathbb{R}^{D \times D}} \\ -\omega_k \mathbb{I}_{\mathbb{R}^{D \times D}} & 0_{\mathbb{R}^{D \times D}} \end{pmatrix}, k \geq 1 \quad (10)$$

Eqn. (1) can now be projected onto the Fourier basis, yielding the harmonic balance equation:

$$A\hat{\mathbf{x}} + \hat{\mathbf{g}}(\hat{\mathbf{x}}) - \hat{\mathbf{e}} = 0_{\mathbb{R}^{(2N+1)D}} \quad (11)$$

where $\hat{\mathbf{e}}$ is defined as in Eqn. (5), and the other terms are explained below.

2.2.1 Linear terms The projection of $\mathscr{L}[\mathbf{x}]$ onto the Fourier basis results in a matrix multiplication $A\hat{\mathbf{x}}$, where $A \in \mathbb{R}^{(2N+1)D \times (2N+1)D}$ is block-diagonal. Furthermore $A = A_{ml} + A_c$, where A_{ml} and A_c are both block-diagonal, and correspond to the linear memoryless and convolution terms, respectively.

$A_{ml}\hat{\mathbf{x}}$ corresponds to the memoryless part $\mathscr{L}_{ml}$ of the linear terms:

$$A_{ml} = \begin{pmatrix} A_{ml_0} & & 0 \\ & \ddots & \\ 0 & & A_{ml_N} \end{pmatrix} \quad (12)$$

with $A_{ml_0} = S \in \mathbb{R}^{D \times D}$, and

$$A_{ml_k} = \begin{pmatrix} -\omega_k^2 M + S & \omega_k C \\ -\omega_k C & -\omega_k^2 M + S \end{pmatrix} \in \mathbb{R}^{2D \times 2D}, k \geq 1 \quad (13)$$

$A_c\hat{\mathbf{x}}$ corresponds to the radiation convolution integral $\mathscr{L}_c$ which, using Ogilvie's relation [12], simplifies into a simple frequency-wise multiplication, involving the frequency-domain representation of the convolution kernel K. More specifically, introducing the infinite-frequency added mass M_∞, and the frequency-dependent added mass and damping matrices $M_\text{a}(\omega)$ and $B(\omega) \in \mathbb{R}^{D \times D}$, A_c can be written as:

$$A_c = \begin{pmatrix} A_{c_0} & & 0 \\ & \ddots & \\ 0 & & A_{c_N} \end{pmatrix} \quad (14)$$

with $A_{c_0} = 0_{\mathbb{R}^{D \times D}}$, and

$$A_{c_k} = \begin{pmatrix} -\omega_k^2(M_a(\omega_k) - M_\infty) & \omega_k B(\omega_k) \\ -\omega_k B(\omega_k) & -\omega_k^2(M_a(\omega_k) - M_\infty) \end{pmatrix} \in \mathbb{R}^{2D \times 2D}, k \geq 1 \tag{15}$$

Note that, in the above expression, some rows and columns of M_∞, $M_a(\omega)$ and $B(\omega)$ may be zeros, when the corresponding rows and columns of $K(\tau)$ are zeros.

2.2.2 Non-linear terms $\hat{\mathbf{g}}(\hat{\mathbf{x}})$ represents the projection, onto the Fourier basis, of the non-linear terms $\mathbf{g}(\mathbf{x}, \dot{\mathbf{x}}, \ddot{\mathbf{x}})$, so that

$$\hat{\mathbf{g}}(\hat{\mathbf{x}}) = \begin{pmatrix} \hat{\mathbf{g}}_0(\hat{\mathbf{x}}) \\ \vdots \\ \hat{\mathbf{g}}_{2N}(\hat{\mathbf{x}}) \end{pmatrix} \in \mathbb{R}^{(2N+1)D} \tag{16}$$

where

$$\hat{\mathbf{g}}_0(\hat{\mathbf{x}}) = \frac{1}{T} \int_0^T \mathbf{g}(\mathbf{x}(t), \dot{\mathbf{x}}(t), \ddot{\mathbf{x}}(t)) dt$$

$$\forall k \in \{1...N\} \begin{cases} \hat{\mathbf{g}}_{2k-1}(\hat{\mathbf{x}}) = \frac{2}{T} \int_0^T \mathbf{g}(\mathbf{x}(t), \dot{\mathbf{x}}(t), \ddot{\mathbf{x}}(t)) \cos(\omega_i t) dt \\ \hat{\mathbf{g}}_{2k}(\hat{\mathbf{x}}) = \frac{2}{T} \int_0^T \mathbf{g}(\mathbf{x}(t), \dot{\mathbf{x}}(t), \ddot{\mathbf{x}}(t)) \sin(\omega_i t) dt \end{cases} \tag{17}$$

and where $\hat{\mathbf{x}}$ and $\mathbf{x}$ are related as in Eqn. (7).

In the absence of non-linear terms, Eqn. (11) simplifies into the usual linear frequency-domain formulation, $A\hat{\mathbf{x}} - \hat{\mathbf{e}} = 0$ [13]. Otherwise, Eqn. (11) is a non-linear vector equation, which is typically solved using gradient-based techniques [6]. The main advantage of Eqn. (11), with respect to Eqn. (1), is that the memory terms simplify, and are represented in a sparse matrix form, along with other linear terms, without requiring any approximation. The non-linear terms remain calculated in the time-domain, which ensures accurate results, provided that the number of harmonics is chosen sufficiently large [6].

3 THE ISWEC DEVICE
3.1 Working principle
The ISWEC (Inertial Sea Wave Energy Converter) is a device that produces energy from sea waves, by exploiting the gyroscopic effect, generated by the combination of the pitch motion of the floater and the rotation of a flywheel. Its working principle is described in [10], and is briefly summarised here for convenience.
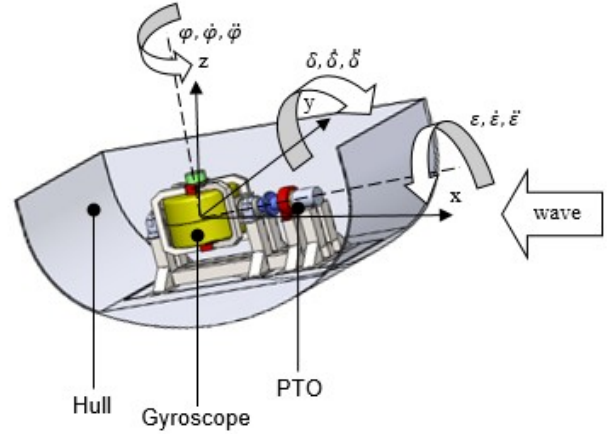

FIGURE 1. ISWEC floater and gyroscopic system scheme - reproduced from [10]

The dynamics of the system can be described using two coordinate systems having the same origin, as shown in Fig. 1. The first one, (x, y, z), is attached to the hull, and is represented by solid lines, while the second one, (x', y', z'), rotates with the gyroscope structure and is shown with dashed lines.

Fig. 1 also illustrates the main system components: the hull, the gyroscope (with its frame) and the PTO. The hull is completely sealed and isolates all the mechanical components from the external environment. The gyroscope system consists of a flywheel and a frame. Sea waves induce a pitch motion δ on the hull. The flywheel rotates around the z' axis with angular speed $\dot{\varphi}$ which, combined with the motion of the hull, generates a gyroscopic torque acting on the gyroscope frame, about the PTO axis x'. As a result, the entire gyroscope rotates with angular speed $\dot{\varepsilon}$ about the PTO axis.

3.2 Dynamical equations
Although the ISWEC captures energy from pitch motion, in practice the floater is also allowed to move in the other hydrodynamic DoFs, in particular heave and surge. However, for the sake of simplicity, both heave and surge are neglected in the model chosen for the purposes of this paper. There are then two DoFs considered: one for the hull (pitch, denoted δ), and one for the gyroscopic system (rotation about the PTO axis, denoted ε).

The simplified analytic model for the device motion is taken from [10]. The Cummins' equation for the pitch motion of the hull is written as:

$$(I_{eq} + \mu_\infty)\ddot{\delta} + \int_0^t h(t - \tau)\dot{\delta}(\tau)d\tau + \beta|\dot{\delta}|\dot{\delta}$$
$$+ s_w \delta - J_g \dot{\varphi}\dot{\varepsilon}\cos(\varepsilon) = T_w \tag{18}$$

where T_w is the torque induced on the floater by the waves, I_{eq} is the moment of inertia of the device for pitch, μ_∞ is the infinite added mass, $\int_0^t h(t-\tau)\dot{\delta}(\tau)d\tau$ is the convolution integral of radiation forces, β is a quadratic viscous damping coefficient, and s_w is the linear hydrostatic stiffness. The last term on the left-hand side of the equation represents the pitch torque generated by the gyroscopic system on the hull, where J_g is the flywheel moment of inertia about its rotating axis.

The gyroscope motion is described by the following equation:

$$I_g\ddot{\varepsilon} + J_g\dot{\varphi}\dot{\delta}cos(\varepsilon) = T_\varepsilon \tag{19}$$

where I_g is the overall gyroscope moment of inertia around the precession axis, and the term $J_g\dot{\varphi}\dot{\delta}cos(\varepsilon)$ non-linearly couples the gyroscope dynamics with the pitch motion. The PTO control torque T_ε consists of two parts: a stiffness component proportional to the angular position ε about the PTO axis, and a damping component proportional to the angular speed $\dot{\varepsilon}$, so that:

$$T_\varepsilon = k_{PTO}\varepsilon + c_{PTO}\dot{\varepsilon} \tag{20}$$

Eqns. (18), (19) and (20) are combined to obtain:

$$\begin{cases} (I_{eq}+\mu_\infty)\ddot{\delta}+s_w\delta+\int_0^t h(t-\tau)\dot{\delta}(\tau)d\tau+ \\ \qquad +\beta|\dot{\delta}|\dot{\delta}-J_g\dot{\varphi}\dot{\varepsilon}cos(\varepsilon)-T_w=0 \\ I_g\ddot{\varepsilon}+c_{PTO}\dot{\varepsilon}+k_{PTO}\varepsilon+J_g\dot{\varphi}\dot{\delta}cos(\varepsilon)=0 \end{cases} \tag{21}$$

A more complete dynamical description would involve a third equation, to describe the equilibrium of the flywheel around its axis φ [14]. As shown in [14], the values of the inertial torques exchanged around this axis are orders of magnitudes smaller with respect to the torques exchanged around the ε and δ axis. Moreover the large inertia of the flywheel filters the inertial torques leading to a quasi-constant flywheel speed.

Finally, a linearised model is also built, as explained in [9], which is used for the initialisation of the HB algorithm.

4 HARMONIC BALANCE IMPLEMENTATION OF THE ISWEC MODEL

Eqn. (21) is in the form of Eqns. (1)-(4), where:

- the number of DoFs is $D=2$, and $\mathbf{x}(t) = \begin{pmatrix} \delta(t) \\ \varepsilon(t) \end{pmatrix}$

- the excitation terms are $\mathbf{e}(t) = \begin{pmatrix} T_w(t) \\ 0 \end{pmatrix}$

- the linear memoryless coefficients of $\mathscr{L}_{ml}$ are given as:

$$M = \begin{pmatrix} I_{eq}+\mu_\infty & 0 \\ 0 & I_g \end{pmatrix}, C = \begin{pmatrix} 0 & 0 \\ 0 & c_{PTO} \end{pmatrix}, S = \begin{pmatrix} s_w & 0 \\ 0 & k_{PTO} \end{pmatrix}$$

- the linear convolution kernel of $\mathscr{L}_c$ is $K(\tau) = \begin{pmatrix} h(\tau) & 0 \\ 0 & 0 \end{pmatrix}$

- the non-linear terms are given as:

$$\mathscr{N}[\mathbf{x}] = \mathbf{g}(\mathbf{x},\dot{\mathbf{x}},\ddot{\mathbf{x}}) = \begin{pmatrix} \beta|\dot{\delta}|\dot{\delta}-J_g\dot{\varphi}\dot{\varepsilon}cos(\varepsilon) \\ J_g\dot{\varphi}\dot{\delta}cos(\varepsilon) \end{pmatrix}$$

Finally, the transcription of Eqn. (21) into the HB problem of Eqn. (11) requires to express the linear terms in matrix form, using M, C, S and K. For the model considered, following the steps detailed in Section 2.2.1 yields

$$A = \begin{pmatrix} A_0 & & 0 \\ & \ddots & \\ 0 & & A_N \end{pmatrix} \tag{22}$$

with $A_0 = \begin{pmatrix} s_w & 0 \\ 0 & k_{PTO} \end{pmatrix}$, and for $k \geq 1$, $A_k = \begin{pmatrix} A_k^{11} & A_k^{12} \\ -A_k^{12} & A_k^{11} \end{pmatrix}$ with:

$$A_k^{11} = \begin{pmatrix} -\omega_k^2(I_{eq}+M_a(\omega_k))+s_w & 0 \\ 0 & -\omega_k^2 I_g + k_{PTO} \end{pmatrix}$$

$$A_k^{12} = \begin{pmatrix} \omega_k B(\omega_k) & 0 \\ 0 & \omega_k c_{PTO} \end{pmatrix}$$

where $M_a(\omega)$ and $B(\omega)$ are the frequency-dependent radiation added-mass and damping for the hull in pitch motion.

The fundamental frequency ω_1 is chosen as $2\pi/T$, where T is the period of the excitation signal. In contrast, the number of harmonics, N, chosen for the HB problem formulation, depends on the case considered (especially the harmonic content of the wave excitation input, and the level of non-linearity in the system). The issue of the choice of N is discussed in Section 5 on a case-by-case basis.

For the numerical examples studied in this paper, Eqn. (11) is solved using a trust-region algorithm, available in the *fsolve* function of Matlab[2]. The Jacobian of $A\hat{\mathbf{x}}+\hat{\mathbf{g}}(\hat{\mathbf{x}})$ is explicitly calculated, which significantly improves the computational performance of the technique. The details of the gradient computation are not developed in this paper, but the method employed is very similar to the one studied in the appendix of [6].

_____

[2]https://uk.mathworks.com/

The starting point $\hat{\mathbf{x}}^{(0)}$ of the root-finding algorithm is important for the computational performance of the HB method. In this paper, the ISWEC linearised model is used (see [9]), and $\hat{\mathbf{x}}^{(0)}$ is found by solving $A'\hat{\mathbf{x}} = \hat{\mathbf{e}}$, where A', similarly to A, expresses the terms of the linearised model in the frequency domain.

5 NUMERICAL RESULTS

In this section, the suitability of the HB method for the analysis of the ISWEC device is investigated, in both regular and irregular waves. RK2 simulations are also used as a point of comparison, for a better understanding of the HB properties.

5.1 Regular waves

A range of monochromatic wave conditions is defined, based on the scatter diagram at the site of Pantelleria island (the design location of the ISWEC device), which can be found, for example, in [15]. The (H_s, T_e) conditions at the Pantelleria site are "converted" into monochromatic wave signals $\eta(t) = A\cos(\frac{2\pi}{T}t)$, with period $T = T_e$, and amplitude $H = 2A$ such that the signal variance, m_0, is identical for the polychromatic and the monochromatic wave signals, that is $m_0 = H_s^2/16 = H^2/8$ so that $H = H_s/\sqrt{2}$.

The control parameters $(c_{PTO}, k_{PTO}, \dot{\varphi})$ have been optimised in previous work at Politecnico di Torino [9, 10] for each (H_s, T_e) couple. Therefore, the appropriate settings for $(c_{PTO}, k_{PTO}, \dot{\varphi})$, in a given monochromatic (H, T) condition, are chosen based on the optimised values in the corresponding polychromatic (H_s, T_e) condition.

With the HB method for a regular wave signal of period T, the fundamental frequency can be simply chosen as $\omega_1 = 2\pi/T$. Then, the number N of harmonics $\omega_k = k\omega_1$ must be chosen, knowing that the accuracy of the HB results improves exponentially with N [7]. Running the HB method with different numbers of harmonics ($N = \{2, 3, 6, 9, 12, 15\}$) in all wave conditions, it is found that:

- A higher excitation level involves more significant nonlinear effects, and hence requires a higher number of harmonics;
- However, in all cases considered, there is no perceptible change in the results beyond $N = 6$.

The two points above are illustrated in Fig. 2, where the peak-to-trough amplitude of the solution ε is plotted for different values of N, for a wave period $T = 6$s and two excitation levels, $H = 1$m and $H = 1.5$m. The asymptotic value ($N \to \infty$) is approximated as the value for $N = 15$. It can be seen that for $H = 1.5$m, a small number of harmonics, $N < 6$, results in a small but noticeable inaccuracy with respect to the asymptotic value.

RK2 simulations of the physical model in Eqn. (21) are also carried out, with different integration time-steps. Unlike the HB
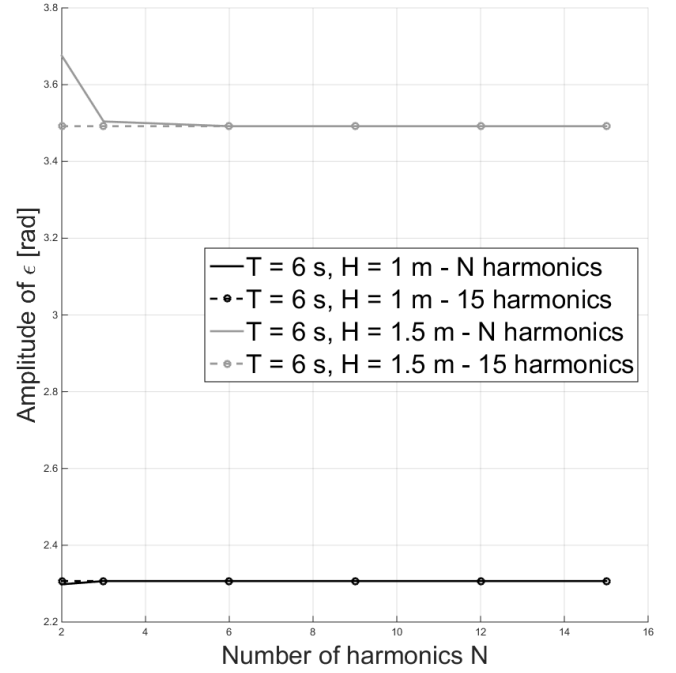

FIGURE 2. Peak-to-trough amplitude of the solution ε, obtained through HB with different numbers of harmonics, in regular waves with period $T = 6$s and heights $H = 1$m and $H = 1.5$m. Note that for the case with $H = 1$m, the differences between results obtained with the increasing number of harmonics are virtually undistinguishable.

method which converges exponentially, the RK2 method converges linearly to the exact mathematical solution when the time step Δt goes to zero. As a consequence, and similarly to the results presented in [5], when Δt tends to zero, the RK2 solution tends to the HB solution (with $N \geq 6$). However, in the wave conditions considered, $\Delta t = 0.01$s is sufficient to be well within 1% of the asymptotic solution.

Overall, $N = 6$ (for HB) and $\Delta t = 0.01$s (for RK2) are retained for comparison between HB and time-domain results. The discrepancies between HB and RK2 solutions are measured through a root-mean-square error, in %, between the two trajectories, given as:

$$e_{rms} = \sqrt{\frac{\int_{t=0}^{T}(x_{RK2}(t) - x_{HB}(t))^2 dt}{\int_{t=0}^{T}x_{RK2}^2(t)dt}} \times 100 \qquad (23)$$

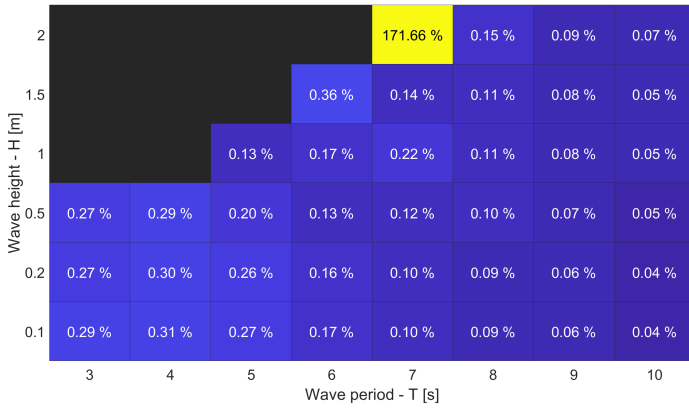where $x_{RK2}(t)$ (resp. $x_{HB}(t)$) are any of the system variables,

FIGURE 3. e_{rms} (%) between HB and RK2 solutions for ε, in a range of regular sea states representative of the Pantelleria island.

e.g. $\delta(t)$ or $\varepsilon(t)$, as obtained with RK2 (resp. HB). Obviously, for RK2, the steady-state of each simulation has to be isolated from the transient, while HB directly solves for the steady-state response.

Fig. 3 shows e_{rms} for the ε variable (which is the most directly related to power absorption), in the whole range of regular wave conditions considered. It can be seen that the HB and time-domain results virtually coincide almost everywhere ($e_{rms} < 0.4\%$), except for the pair ($H = 2$m, $T = 7$s), located at the edge of the studied range of regular wave conditions, and which deserves further investigation.
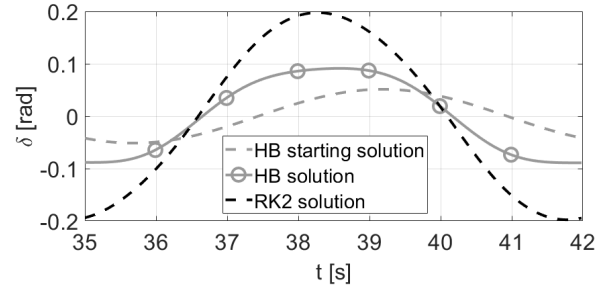
In fact, HB does not converge (at least within a reasonable amount of time) in ($H = 2$m, $T = 7$s) with $N = 6$, but converges with $N \leq 4$. However, the resulting solution is significantly different from the RK2 one (see Fig. 4(a)). Therefore, another starting solution for the HB algorithm is investigated: a shifted and scaled version of the RK2 solution is used as $\hat{\mathbf{x}}^0$ for the HB root-finding algorithm, and this time, HB yields the same solution as RK2 integration (Fig. 4(b)). The results highlighted in Fig. 4 are interesting, because they illustrate that:

- the approximate problem of Eqn. (11) can have multiple solutions, some of which may not have any physical meaning;
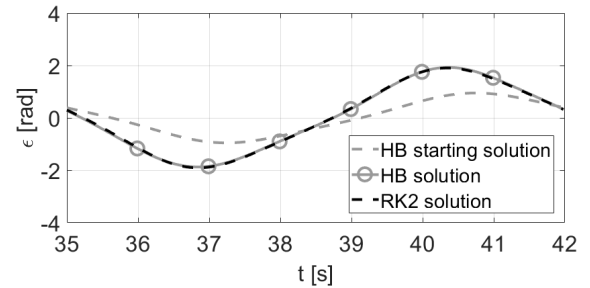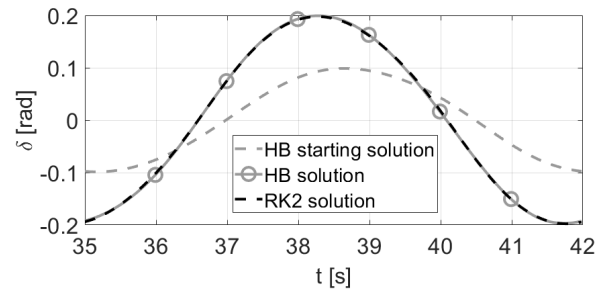- HB results can be sensitive to the algorithm starting point.

5.2 Irregular waves

Next, HB is used for ISWEC simulations in irregular waves, in a range of JONSWAP spectra [16] consistent with the scatter table at Pantelleria island [15].

In contrast to Section 5.1, where the simulation time was adjusted to the wave period, in this section it is chosen to keep a constant simulation time of 120s across the sea states. Therefore,

(a) HB starting from the solution of the linearised model

(b) HB starting from an initial solution closer to the RK2 solution

FIGURE 4. $T = 7$s and $H = 2$m - comparison between results obtained from RK2 and HB ($N = 4$) starting from two different initial solutions.

$\omega_1 = 2\pi/120 \approx 0.05$ rad.s^{-1}. Similarly to the regular wave case study, the convergence of HB with the number of harmonics is investigated. Instead of using the solution amplitude (not well-
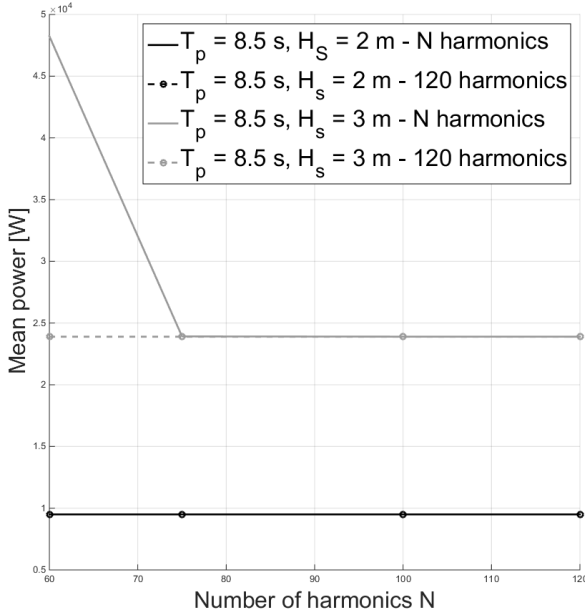
FIGURE 7. ($T_p = 8.5$s, $H_s = 2.5$m): linearised solution for $\mathbf{e}^{mod}(t) = 0.75\mathbf{e}(t)$, and HB non-linear solution $\delta^{mod}(t)$; $\delta^{mod}(t)$ is then used as initial solution to obtain $\delta(t)$

FIGURE 5. Peak-to-trough amplitude of the solution ε, obtained through HB with different numbers of harmonics, in regular waves with period $T = 6$s and heights $H_s = 2$m and $H_s = 3$m. Note that for the case with $H = 2$m, the differences between results obtained with the increasing number of harmonics are virtually undistinguishable.

defined in irregular waves), the mean absorbed power is used to compare the different results. It is found that, in the vast majority of cases, $N = 75$ is sufficient for accurate power assessment in the simulated 120s signal, as illustrated in Fig. 5 for a peak wave period of $T_p = 8.5$s and significant wave heights $H_s = 2$m and $H_s = 3$m respectively. As in the monochromatic case, it can be seen that a larger excitation implies larger non-linear effects, and thus makes it necessary to use more harmonics to obtain accurate results.

As far as RK2 is concerned, a time step $\Delta t = 0.01$s is also found appropriate. A comparison between HB and RK2 results, based on the root-mean-square difference of the solution ε signals, is shown in Fig. 6. In the vast majority of cases, there is good agreement between HB and RK2 results, the e_{rms} generally being lower than 1%.

However, in two cases, namely ($T_p = 6.5$s, $H_s = 2$m) and ($T_p = 8$s, $H_s = 2.5$m), a higher number of harmonics ($N = 120$) must be used to obtain convergence of HB to an accurate solution within a reasonable amount of time. In eight other cases (indicated by $e_{rms} = 100\%$), the HB algorithm does not converge (again, within a reasonable amount of time) when starting from the solution of the linearised model. However, in most of the
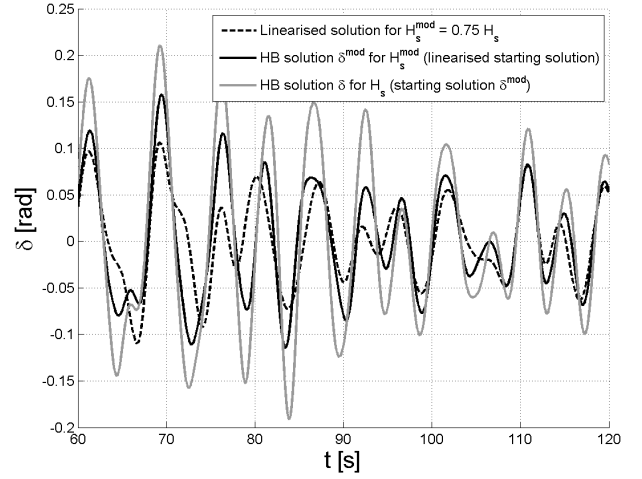
problematic cases, it seems possible to obtain HB convergence by using a more appropriate choice of initial solution. In particular, the following procedure can be applied:

- run HB with a lower excitation level, say $\mathbf{e}^{mod}(t) = 0.75\mathbf{e}(t)$, for which HB converges; save the solution, say $\hat{\mathbf{x}}^{mod}$;
- run HB with $\mathbf{e}(t)$ and using $\hat{\mathbf{x}}^{mod}$ as starting solution.

The above method is illustrated in Fig. 7. It can be iterated several times if necessary, and extends the range of cases where HB converges.

6 CONCLUSION

The formalism developed in Section 2, for HB implementation in the scope of non-linear WEC simulation, is applicable to a wide range of dynamical models, whether they only describe hydrodynamic interactions or also include internal PTO dynamics, and whether the WEC system considered is a single device or consists of an array.

A 2-DoF model of the ISWEC device is chosen as an application example, as explained in Section 3. The first DoF is the pitching motion of the device, subject to hydrodynamic interaction with incoming waves, while the second DoF describes the rotation of the internal gyroscope system, which is the DoF along which mechanical power is converted to electrical power. The equations describing the hull motion and the gyroscope dynamics are coupled through non-linear terms. The implementation of the HB method for the specific model considered is detailed in Section 4.
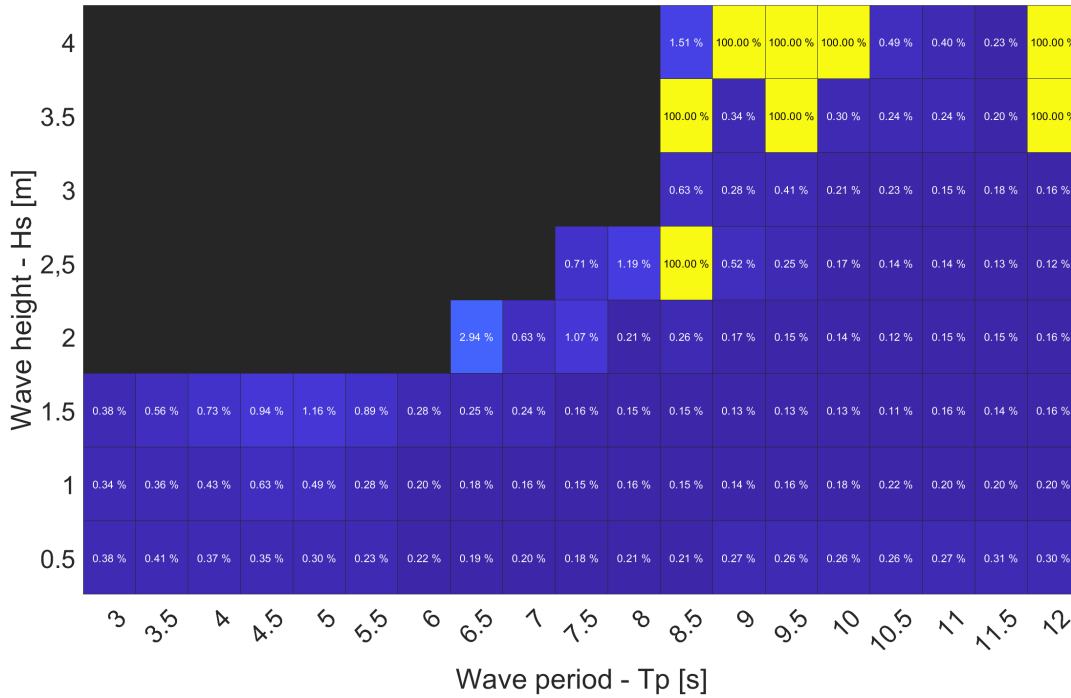
FIGURE 6. e_{rms} (%) between HB and RK2 solutions for ε, in a range of irregular sea states representative of the Pantelleria island. Cells with e_{rms} in the order of 100% are those where the HB algorithm does not converge within a reasonable amount of time.

The numerical results of Section 5.1 show the suitability of HB to study strongly non-linear, multi-DoF WEC motions in regular and irregular waves. In particular, the exponential convergence of HB towards the exact steady-state mathematical solution is illustrated. In regular waves, only one wave period needs to be simulated and, in spite of the strong non-linearities, a relatively small number of harmonics (here, $N = 6$) is sufficient for accurate results. In irregular waves, the relevant number of harmonics is significantly larger, due to the necessarily long simulation time, but exponential convergence of HB results can also be observed.

Although issues related to computation time have not been discussed in detail in this paper, gains of between one and two orders of magnitude can be expected with respect to RK2. Furthermore, the HB formalism can allow for solving multiple problems in only one run, thus resulting in additional computational savings. The latter possibility will be explored in future work by the authors.

However, unlike time-domain integration, the HB method is sensitive to the algorithm starting point. In some specific cases (especially in highly energetic seas, both regular and irregular), the HB root-finding algorithm may fail to converge, when starting from the solution of the linearised system. Different ways

could be considered to deal with convergence issues:

- the solution of a *neighbouring* problem, also obtained with HB, could be used as a starting point, as suggested in Section 5.2;
- given that the typical wave conditions, in which convergence issues occur, only represent a tiny fraction of the overall annual wave conditions at the site considered [17], time-domain integration could be used as a last-resort solution when HB fails to converge.

Another issue with potentially significant implications is the existence, in some cases, of multiple solutions to the HB equation. It should be useful to investigate ways to detect non-physical solutions. For example, a solution could be considered "suspicious" if, by a small change in the control parameters or wave elevation, the results change significantly. Alternatively, tools from Floquet analysis [18] (to assess the stability of a trajectory of a non-linear system) could be put to good use.

Overall, as far as the application of HB to the ISWEC device is concerned, the HB method could be used to refine the tuning of the ISWEC control parameters, taking into account a more accurate representation of non-linear effects in the device dynamics, or to carry out detailed power assessment in various locations.

More work would then be needed, to determine the appropriate length and number of HB simulation to be run for each sea state to obtain representative results [19].

REFERENCES

[1] Folley, M., 2016. *Numerical Modelling of Wave Energy Converters*. Academic Press.

[2] Penalba Retes, M., Mérigaud, A., Gilloteaux, J.-C., and Ringwood, J., 2015. "Nonlinear froude-krylov force modelling for two heaving wave energy point absorbers". In Proceedings of the 11th European Wave and Tidal Energy Conference, European Wave and Tidal Energy Conference 2015.

[3] Armesto, J. A., Guanche, R., Del Jesus, F., Iturrioz, A., and Losada, I. J., 2015. "Comparative analysis of the methods to compute the radiation term in cummins equation". *Journal of Ocean Engineering and Marine Energy, 1*(4), pp. 377–393.

[4] Folley, M., and Whittaker, T., 2010. "Spectral modelling of wave energy converters". *Coastal Engineering, 57*(10), pp. 892–897.

[5] Mérigaud, A., and Ringwood, J. V., 2018. "A nonlinear frequency-domain approach for numerical simulation of wave energy converters". *IEEE Transactions on Sustainable Energy, 9*(1), pp. 86–94.

[6] Mukundan, L., 1991. "Convergence analysis for the harmonic balance method". PhD thesis, North Carolina State University.

[7] Nastov, O. J., 1999. "Spectral methods for circuit analysis". PhD thesis, Massachusetts Institute of Technology.

[8] Mérigaud, A., and Ringwood, J. V., 2017. "Non-linear frequency-domain wec simulation: Numerical case studies and practical issues". In Proceedings of the 11th European Wave and Tidal Energy Conference, Cork, Ireland.

[9] Sirigu, S. A., Vissio, G., Bracco, G., Giorcelli, E., Passione, B., Raffero, M., and Mattiazzo, G., 2016. "Iswec design tool". *International Journal of Marine Energy, 15*, pp. 201–213.

[10] Vissio, G., Bracco, G., Giorcelli, E., Mattiazzo, G., Valerio, D., and Beirao, P., 2016. "Iswec control tuning: lessons learned". In Progress in Renewable Energies Offshore: Proceedings of the 2nd International Conference on Renewable Energies Offshore (RENEW2016), Lisbon, Portugal, 24-26 October 2016, CRC Press, p. 427.

[11] Cummins, W., 1962. "The impulse response function and ship motion". *Schiffstechnik*(9), pp. 101–109.

[12] Ogilvie, T., 1964. "Recent progress toward the understanding and prediction of ship motions.". In Sixth Symposium on Naval Hydrodynamics.

[13] Falnes, J., 2002. *Ocean waves and oscillating systems: linear interactions including wave-energy extraction*. Cambridge University Press.

[14] Bracco, G. Iswec: A gyroscopic wave energy converter.

[15] Cagninei, A., Raffero, M., Bracco, G., Giorcelli, E., Mattiazzo, G., and Poggi, D., 2015. "Productivity analysis of the full scale inertial sea wave energy converter prototype: A test case in pantelleria island". *Journal of Renewable and Sustainable Energy, 7*(6), p. 061703.

[16] Hasselmann, K., Barnett, T., Bouws, E., Carlson, H., Cartwright, D., Enke, K., Ewing, J., Gienapp, H., Hasselmann, D., Kruseman, P., et al., 1973. Measurements of wind-wave growth and swell decay during the Joint North Sea Wave Project (JONSWAP).

[17] Pozzi, N., Castino, A., Vissio, G., Passione, B., Sirigu, S. A., Bracco, G., and Mattiazzo, G., 2017. "Experimental evaluation of different hydrodynamic modelling techniques applied to the iswec".

[18] Khalil, H. K., 1996. *Noninear systems*, Vol. 2.

[19] Mrigaud, A., and Ringwood, J. V., 2018. "Power production assessment for wave energy converters: Overcoming the perils of the power matrix". *Proceedings of the Institution of Mechanical Engineers, Part M: Journal of Engineering for the Maritime Environment, 232*(1), pp. 50–70.